PROCEEDINGS OF SCIENCE

Bottomonium resonances from lattice QCD static-static-light-light potentials

Pedro Bicudo,[a] **Nuno Cardoso,**[a] **Lasse Mueller**[b,*] **and Marc Wagner**[b]

[a] *CeFEMA, Dep. Física, Instituto Superior Técnico, Universidade de Lisboa, Av. Rovisco Pais, 1049-001 Lisboa, Portugal*

[b] *Johann Wolfgang Goethe-Universität Frankfurt am Main, Institut für Theoretische Physik, Max-von-Laue-Straße 1, D-60438 Frankfurt am Main, Germany*

E-mail: bicudo@tecnico.ulisboa.pt, nuno.cardoso@tecnico.ulisboa.pt, lmueller@th.physik.uni-frankfurt.de, mwagner@th.physik.uni-frankfurt.de

We study $I = 0$ quarkonium resonances decaying into pairs of heavy-light mesons using static-static-light-light potentials from lattice QCD. To this end, we solve a coupled channel Schroedinger equation with a confined quarkonium channel and channels with a heavy-light meson pair to compute phase shifts and t-matrix poles for the lightest decay channel. We find results for S-, P-, D- and F-wave-states to discuss in the context of corresponding experimental results, in particular for $\Upsilon(10753)$ and $\Upsilon(10860)$.

The 38th International Symposium on Lattice Field Theory, LATTICE2021 26th-30th July, 2021 Zoom/Gather@Massachusetts Institute of Technology

*Speaker

PoS(LATTICE2021)349

1. Introduction

In this work we study $I = 0$ quarkonium resonances using Lattice QCD string breaking potentials (computed in [1]). In our approach we use the diabatic extension of the Born-Oppenheimer approximation and the unitary emergent wave method. In the first step of the Born-Oppenheimer approximation heavy quarks are regarded as static color charges to compute the potential in presence of two light quarks. In a second step these results are then used as an effective potential in the Schroedinger equation of the heavy quarks. [2]
In the past this approach was already successfully applied to compute resonances for $\bar{b}\bar{b}qq$-systems, where q denotes a light quark of flavor u/d [3]. In this work, we investigate $\bar{b}b\bar{q}q$-systems which on the one hand are in general more complicated due to additional decay channels but on the other hand there are experimental results available in this channel (e.g. $\Upsilon(nS)$, $\Upsilon(10860)$, $\Upsilon(11020)$).
There have also been efforts to study the $I = 1$ isospin-channel in [4].

2. Coupled channel Schroedinger equation

In the following we will construct the Schroedinger equation for our scattering problem. We consider two channels for now, a quarkonium channel $\bar{Q}Q$ and a heavy-light meson-meson channel $\bar{M}M$ with $M = \bar{Q}q$.
We introduce the following quantum numbers:

- J^{PC} : total angular momentum, parity and charge conjugation of the respective system.
- $S^{PC}_{Q/q}$: spin of $\bar{Q}Q/\bar{q}q$ and corresponding parity and charge conjugation.
- $\tilde{J}^{PC}$: total angular momentum excluding the heavy $\bar{Q}Q$ - spins and corresponding parity and charge conjugation. (for Quarkonium $\tilde{J}^{PC}$ coincides with the orbital angular momentum L^{PC} of the two heavy quarks).

We consider heavy quark spins to be conserved quantities. Hence energy levels and other observables will not depend on S^{PC}_{Q}. Note that, since J^{PC} as well as S^{PC}_{Q} are conserved, $\tilde{J}^{PC}$ is also conserved.
In [8] we derived in detail the Schroedinger equation with a 4-component wave function $\psi(\mathbf{r}) = \left(\psi_{\bar{Q}Q}(\mathbf{r}), \vec{\psi}_{\bar{M}M}(\mathbf{r})\right)$. The first component $\psi_{\bar{Q}Q}(\mathbf{r})$ represents the $\bar{Q}Q$-channel, while the three lower components $\vec{\psi}_{\bar{M}M}(\mathbf{r})$ represent the spin-1 triplet of the $\bar{M}M$-channel. The resulting Schroedinger equation reads

$$\left(-\frac{1}{2}\mu^{-1}\left(\partial_r^2 + \frac{2}{r}\partial_r - \frac{\mathbf{L}^2}{r^2}\right) + V(\mathbf{r}) - E\right)\psi(\mathbf{r}) = 0, \tag{1}$$

where $\mu^{-1} = \mathrm{diag}(1/\mu_Q, 1/\mu_M, 1/\mu_M, 1/\mu_M)$ and

$$V(\mathbf{r}) = \begin{pmatrix} V_{\bar{Q}Q} & V_{\mathrm{mix}}(r)\,(1 \otimes \mathbf{e}_r) \\ V_{\mathrm{mix}}(r)\,(\mathbf{e}_r \otimes 1) & V_{\bar{M}M,\parallel}(r)\,(\mathbf{e}_r \otimes \mathbf{e}_r) + V_{\bar{M}M,\perp}(r)\,(1 - \mathbf{e}_r \otimes \mathbf{e}_r) \end{pmatrix}. \tag{2}$$

$V_{\bar{Q}Q}$, V_{mix}, $V_{\bar{M}M,\parallel}$ and $V_{\bar{M}M,\perp}$ can be related to lattice results for static potentials from QCD.

3. Static potentials from lattice QCD

In this section we briefly how the Lattice QCD string beaking potentials from [1] are computed. Heavy quarks are treated as static quarks with frozen positions at $\mathbf{0}$ and $\mathbf{r}$. One can write down operators as trial states for a $\bar{Q}Q$-pair and a meson-meson pair according to

$$O_{Q\bar{Q}} = (\Gamma_Q)_{AB} \qquad \left(\bar{Q}_A(\mathbf{0})\; U(\mathbf{0};\mathbf{r})\; Q_B(\mathbf{r})\right) \tag{3}$$

$$O_{M\bar{M}} = (\Gamma_Q)_{AB}(\Gamma_q)_{CD} \qquad \left(\bar{Q}_A(\mathbf{0})\; u_D(\mathbf{0})\; \bar{u}_C(\mathbf{r})\; Q_B(\mathbf{r}) + (u \to d)\right) \tag{4}$$

One then computes the correlation matrix

$$C(t) = \begin{pmatrix} \langle O_{Q\bar{Q}}|O_{Q\bar{Q}}\rangle_U & \langle O_{Q\bar{Q}}|O_{M\bar{M}}\rangle_U \\ \langle O_{M\bar{M}}|O_{Q\bar{Q}}\rangle_U & \langle O_{M\bar{M}}|O_{M\bar{M}}\rangle_U \end{pmatrix} = \left(\begin{array}{cc} \square & \sqrt{n_f}\;\square \\ \sqrt{n_f}\;\square & -n_f\;\square + \{\} \end{array} \right), \tag{5}$$

The solid lines in Eqn. (5) correspond to gauge transporters while wiggly lines symbolize light quark propagators. The first element of the correlation matrix is a Wilson loop, the off diagonal elements are Wilson loops where one gauge transporter is replaced by a light quark propagator and the last element consists of two more complicated diagrams, one connected and the other one disconnected. From $C(t)$ the potentials can be extracted in the limit of large Euclidean time separations as

$$[C(t)]_{ij} \propto \sum_k a_k(r) \mathrm{e}^{-V_k(r)t} \qquad \text{for} \quad t \to \infty. \tag{6}$$

One can derive a relation between these $V_k(r)$ and $V_{\bar{Q}Q}(r)$, $V_{mix}(r)$ and $V_{\bar{M}M}(r)$ according to

$$\begin{aligned} V_{\bar{Q}Q} &= \cos^2(\theta(r)) V_0^{\Sigma_g^+}(r) + \sin^2(\theta(r)) V_1^{\Sigma_g^+}(r), \\ V_{\bar{M}M,\parallel}(r) &= \sin^2(\theta(r)) V_0^{\Sigma_g^+}(r) + \cos^2(\theta(r)) V_1^{\Sigma_g^+}(r), \\ V_{\mathrm{mix}}(r) &= \cos(\theta(r)) \sin(\theta(r)) \left(V_0^{\Sigma_g^+}(r) + V_1^{\Sigma_g^+}(r) \right), \\ V_{\bar{M}M,\perp}(r) &= V^{\Pi_g^+}(r) = 0, \end{aligned}$$

where $V_0^{\Sigma_g^+}(r)$ denotes the ground state potential and $V_1^{\Sigma_g^+}(r)$ its first excitation. In Fig. 1 we show the data points for $V_{\bar{Q}Q}(r)$, $V_{mix}(r)$ and $V_{\bar{M}M}(r)$ and appropriate parameterizations

$$V_{\bar{Q}Q} = E_0 - \frac{\alpha}{r} + \sigma r + \sum_{j=1}^{2} c_{\bar{Q}Q,j}\, r \exp\left(-\frac{r^2}{2\lambda_{\bar{Q}Q,j}^2} \right), \tag{7}$$

$$V_{\bar{M}M,\parallel}(r) = 0, \tag{8}$$

$$V_{\mathrm{mix}}(r) = \sum_{j=1}^{2} c_{\mathrm{mix},j}\, r \exp\left(-\frac{r^2}{2\lambda_{\mathrm{mix},j}^2} \right). \tag{9}$$

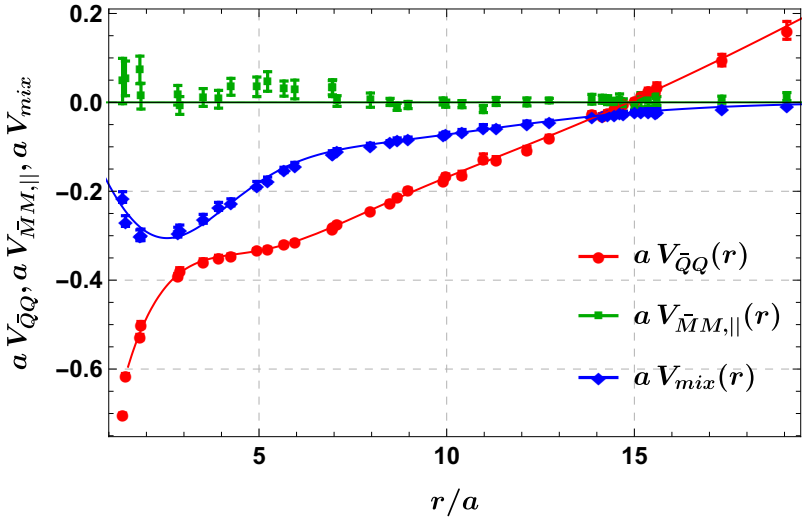

Figure 1: Potentials $V_{\bar{Q}Q}$, $V_{\bar{M}M,\parallel}(r)$ and $V_{\mathrm{mix}}(r)$ as functions of $\bar{Q}Q$ separation r. The curves correspond to the parameterizations (7) to (9) with parameters listed in Table 1.

potential	parameter	value
$V_{\bar{Q}Q}(r)$	E_0	$-1.599(269)$ GeV
	α	$+0.320(94)$
	σ	$+0.253(035)$ GeV^2
	$c_{\bar{Q}Q,1}$	$+0.826(882)$ GeV^2
	$\lambda_{\bar{Q}Q,1}$	$+0.964(47)$ GeV^{-1}
	$c_{\bar{Q}Q,2}$	$+0.174(1.004)$ GeV^2
	$\lambda_{\bar{Q}Q,2}$	$+2.663(425)$ GeV^{-1}
$V_{\bar{M}M,\parallel}(r)$	–	–
$V_{\mathrm{mix}}(r)$	$c_{\mathrm{mix},1}$	$-0.988(32)$ GeV^2
	$\lambda_{\mathrm{mix},1}$	$+0.982(18)$ GeV^{-1}
	$c_{\mathrm{mix},2}$	$-0.142(7)$ GeV^2
	$\lambda_{\mathrm{mix},2}$	$+2.666(46)$ GeV^{-1}

Table 1: The parameters of the potential parametrizations (7) to (9).

4. Scattering matrix for angular momentum $\tilde{J}$

We expand $\psi(\mathbf{r})$ in terms of $\tilde{J}$ eigenfunctions and project the SE to definite angular momentum. For $\tilde{J} > 0$ we receive three coupled equations

$$\left(-\tfrac{1}{2}\mu^{-1}\partial_r^2 + \tfrac{1}{2r^2}L_{\tilde{J}}^2 + V_{\tilde{J}}(r) + \begin{pmatrix} E_{\mathrm{threshold}} & 0 & 0 \\ 0 & 2m_M & 0 \\ 0 & 0 & 2m_M \end{pmatrix} + E\,\mathbb{1}_{3\times 3}\right)\begin{pmatrix} u_{\tilde{J}}(r) \\ \chi_{\tilde{J}-1\to\tilde{J}}(r) \\ \chi_{\tilde{J}+1\to\tilde{J}}(r) \end{pmatrix} =$$

$$= \begin{pmatrix} V_{\mathrm{mix}}(r) \\ 0 \\ 0 \end{pmatrix}\left(\alpha_1 \cdot \tfrac{\tilde{J}}{2\tilde{J}+1}\, kr\, j_{\tilde{J}-1}(kr) + \alpha_2 \cdot \tfrac{\tilde{J}+1}{2\tilde{J}+1}\, kr\, j_{\tilde{J}+1}(kr)\right), \qquad (10)$$

with

$$\mu^{-1} = \text{diag}(\ 1/\mu_Q,\ 1/\mu_M,\ 1/\mu_M), \tag{11}$$

$$L^2_{\tilde{J}} = \text{diag}(\ \tilde{J}(\tilde{J}+1),\ (\tilde{J}-1)\tilde{J},\ (\tilde{J}+1)(\tilde{J}+2)) \tag{12}$$

and

$$V_{\tilde{J}}(r) = \begin{pmatrix} V_{\bar{Q}Q}(r) & \sqrt{\frac{\tilde{J}}{2\tilde{J}+1}}V_{\text{mix}}(r) & \sqrt{\frac{\tilde{J}+1}{2\tilde{J}+1}}V_{\text{mix}}(r) \\ \sqrt{\frac{\tilde{J}}{2\tilde{J}+1}}V_{\text{mix}}(r) & 0 & 0) \\ \sqrt{\frac{\tilde{J}+1}{2\tilde{J}+1}}V_{\text{mix}}(r) & 0 & 0 \end{pmatrix}. \tag{13}$$

The incoming wave can be any superposition of a $\bar{B}^{(*)}B^{(*)}$ wave with $L = \tilde{J}-1$ and a $\bar{B}^{(*)}B^{(*)}$ wave with $L = \tilde{J}+1$. E. g. a pure incoming $\bar{B}^{(*)}B^{(*)}$ wave with $L = \tilde{J}-1$ translates to $(\alpha_1, \alpha_2) = (1, 0)$. The boundary conditions are the following:
For all cases

$$u_{\tilde{J}}(r) \propto r^{\tilde{J}-1} \quad \text{and} \quad \chi_{L\to\tilde{J}}(r) \propto r^{L-1} \qquad \text{for} \quad r \to 0, \tag{14}$$

$$u_{\tilde{J}}(r) = 0 \qquad \text{for} \quad r \to \infty, \tag{15}$$

for $\boldsymbol{\alpha} = (1, 0)$

$$\chi_{\tilde{J}-1\to\tilde{J}}(r) = it_{\tilde{J}-1,\tilde{J}-1}\, kr\, h^{(1)}_{\tilde{J}-1}(kr), \qquad \chi_{\tilde{J}+1\to\tilde{J}}(r) = it_{\tilde{J}-1,\tilde{J}+1}\, kr\, h^{(1)}_{\tilde{J}+1}(kr) \quad \text{for} \quad r \to \infty, \tag{16}$$

and for $\boldsymbol{\alpha} = (0, 1)$

$$\chi_{\tilde{J}-1\to\tilde{J}}(r) = it_{\tilde{J}+1,\tilde{J}-1}\, kr\, h^{(1)}_{\tilde{J}-1}(kr), \qquad \chi_{\tilde{J}+1\to\tilde{J}}(r) = it_{\tilde{J}+1,\tilde{J}+1}\, kr\, h^{(1)}_{\tilde{J}+1}(kr) \quad \text{for} \quad r \to \infty. \tag{17}$$

This defined the matrices $T_{\tilde{J}}$ and $S_{\tilde{J}}$,

$$T_{\tilde{J}} = \begin{pmatrix} t_{\tilde{J}-1,\tilde{J}-1} & t_{\tilde{J}+1,\tilde{J}-1} \\ t_{\tilde{J}-1,\tilde{J}+1} & t_{\tilde{J}+1,\tilde{J}+1} \end{pmatrix}, \quad S_{\tilde{J}} = 1 + 2iT_{\tilde{J}}. \tag{18}$$

Note that, the corresponding coupled channel Schroedinger equation for $\tilde{J} = 0$ is obtained by discarding the central equation of Eqn. (10). As a consequence, the scattering matrix in this case is just a scalar $t_{1,1}$.
We now computed the masses and decay widths of resonances by finding poles of $T_{\tilde{J}}$ in the complex energy plane. Unfortunately, the results show large discrepancies to the mass spectrum from experiment. In order to improve our approach, we include an additional $\bar{B}^{(*)}_s B^{(*)}_s$-channel.

5. Extension by a $\bar{B}^{(*)}_s B^{(*)}_s$-channel

In this approach we are able to compute meaningful results for energies between the $\bar{B}^{(*)}B^{(*)}$-threshold of two parity negative mesons at 10.627 and the $\bar{B}^{(*)}B^{(*)}$-threshold of one parity negative

and one parity positive meson at 11.020. The $\bar{B}_s^{(*)}B_s^{(*)}$-threshold of two parity negative mesons is at 10.807, thus, we expect a significant improvement on our results when including an additional $\bar{B}_s^{(*)}B_s^{(*)}$-channel.

We use the same string breaking potentials from [1]. We expect this to be reasonable since the light quark mass used in the lattice data is between the physical u/d quark mass and the physical s quark mass. As a consistency check we compared the eigenvalues of the resulting 3×3 potential matrix for $\tilde{J} = 0$ and found that they compare well to the three lowest energy level computed by a recent lattice computation with a system of a heavy quark-antiquark pair and dynamical u, d and s quarks [5]. For a more detailed discussion see our recent work [6].

The Schroedinger equation with the additional $\bar{B}_s^{(*)}B_s^{(*)}$-channel now reads

$$\left(\frac{1}{2}\mu^{-1}\,\partial_r^2 + \frac{1}{2r^2}L_{\tilde{J}}^2 + V_{\tilde{J}}(r) + \right. \tag{19}$$
$$\left. + \begin{pmatrix} E_{\text{threshold}} & 0 & 0 & 0 & 0 \\ 0 & 2m_M & 0 & 0 & 0 \\ 0 & 0 & 2m_M & 0 & 0 \\ 0 & 0 & 0 & 2m_{M_s} & 0 \\ 0 & 0 & 0 & 0 & 2m_{M_s} \end{pmatrix} - E\;\mathbb{1}_{5\times 5} \right) \begin{pmatrix} u_{\tilde{J}}(r) \\ \chi_{\bar{M}M,\tilde{J}-1\to\tilde{J}}(r) \\ \chi_{\bar{M}M,\tilde{J}+1\to\tilde{J}}(r) \\ \chi_{\bar{M}_sM_s,\tilde{J}-1\to\tilde{J}}(r) \\ \chi_{\bar{M}_sM_s,\tilde{J}+1\to\tilde{J}}(r) \end{pmatrix} =$$
$$= \begin{pmatrix} V_{\text{mix}}(r) \\ 0 \\ 0 \\ 0 \\ 0 \end{pmatrix} \left(\alpha_{\bar{M}M,1}\,\frac{\tilde{J}}{2\tilde{J}+1}\,kr\,j_{\tilde{J}-1}(kr) + \alpha_{\bar{M}M,2}\,\frac{\tilde{J}+1}{2\tilde{J}+1}\,kr\,j_{\tilde{J}+1}(kr) + \right.$$
$$\left. + \alpha_{\bar{M}_sM_s,1}\,\frac{\tilde{J}}{2\tilde{J}+1}\,k_sr\,j_{\tilde{J}-1}(k_sr)/\sqrt{2} + \alpha_{\bar{M}_sM_s,2}\,\frac{\tilde{J}+1}{2\tilde{J}+1}\,k_sr\,j_{\tilde{J}+1}(k_sr)/\sqrt{2} \right), \tag{20}$$

where

$$\mu^{-1} = \text{diag}(\,1/\mu_Q,\;1/\mu_M,\;1/\mu_M,\;1/\mu_{M_s},\;1/\mu_{M_s}\,), \tag{21}$$
$$L_{\tilde{J}}^2 = \text{diag}(\,\tilde{J}(\tilde{J}+1),\;(\tilde{J}-1)\tilde{J},\;(\tilde{J}+1)(\tilde{J}+2),\;(\tilde{J}-1)\tilde{J},\;(\tilde{J}+1)(\tilde{J}+2)\,) \tag{22}$$

and

$$V_{\tilde{J}}(r) = \begin{pmatrix} V_{\bar{Q}Q}(r) & \sqrt{\frac{\tilde{J}}{2\tilde{J}+1}}V_{\text{mix}}(r) & \sqrt{\frac{\tilde{J}+1}{2\tilde{J}+1}}V_{\text{mix}}(r) & \frac{1}{\sqrt{2}}\sqrt{\frac{\tilde{J}}{2\tilde{J}+1}}V_{\text{mix}}(r) & \frac{1}{\sqrt{2}}\sqrt{\frac{\tilde{J}+1}{2\tilde{J}+1}}V_{\text{mix}}(r) \\ \sqrt{\frac{\tilde{J}}{2\tilde{J}+1}}V_{\text{mix}}(r) & 0 & 0 & 0 & 0 \\ \sqrt{\frac{\tilde{J}+1}{2\tilde{J}+1}}V_{\text{mix}}(r) & 0 & 0 & 0 & 0 \\ \frac{1}{\sqrt{2}}\sqrt{\frac{\tilde{J}}{2\tilde{J}+1}}V_{\text{mix}}(r) & 0 & 0 & 0 & 0 \\ \frac{1}{\sqrt{2}}\sqrt{\frac{\tilde{J}+1}{2\tilde{J}+1}}V_{\text{mix}}(r) & 0 & 0 & 0 & 0 \end{pmatrix}. \tag{23}$$

With four linear independent choices of $\boldsymbol{\alpha} = (\alpha_{\bar{M}M,1}, \alpha_{\bar{M}M,2}, \alpha_{\bar{M}_sM_s,1}, \alpha_{\bar{M}_sM_s,2})$ and by choosing appropriate boundary conditions analogously to Eqns. (14) to (17) we obtain a 4x4-scattering

matrix

$$T_{\tilde{J}} = \begin{pmatrix} t_{\bar{M}M,\tilde{J}-1;\bar{M}M,\tilde{J}-1} & t_{\bar{M}M,\tilde{J}+1;\bar{M}M,\tilde{J}-1} & t_{\bar{M}_sM_s,\tilde{J}-1;\bar{M}M,\tilde{J}-1} & t_{\bar{M}_sM_s,\tilde{J}+1;\bar{M}M,\tilde{J}-1} \\ t_{\bar{M}M,\tilde{J}-1;\bar{M}M,\tilde{J}+1} & t_{\bar{M}M,\tilde{J}+1;\bar{M}M,\tilde{J}+1} & t_{\bar{M}_sM_s,\tilde{J}-1;\bar{M}M,\tilde{J}+1} & t_{\bar{M}_sM_s,\tilde{J}+1;\bar{M}M,\tilde{J}+1} \\ t_{\bar{M}M,\tilde{J}-1;\bar{M}_sM_s,\tilde{J}-1} & t_{\bar{M}M,\tilde{J}+1;\bar{M}_sM_s,\tilde{J}-1} & t_{\bar{M}_sM_s,\tilde{J}-1;\bar{M}_sM_s,\tilde{J}-1} & t_{\bar{M}_sM_s,\tilde{J}+1;\bar{M}_sM_s,\tilde{J}-1} \\ t_{\bar{M}M,\tilde{J}-1;\bar{M}_sM_s,\tilde{J}+1} & t_{\bar{M}M,\tilde{J}+1;\bar{M}_sM_s,\tilde{J}+1} & t_{\bar{M}_sM_s,\tilde{J}-1;\bar{M}_sM_s,\tilde{J}+1} & t_{\bar{M}_sM_s,\tilde{J}+1;\bar{M}_sM_s,\tilde{J}+1} \end{pmatrix}. \quad (24)$$

Energies at which a component of $T_{\tilde{J}}$ diverges can be related to masses and decay widths of resonances.

6. Results

We consider the analytic continuation of our scattering problem into the complex energy plane, where we search for poles in the of $T_{\tilde{J}}$ by using a Newton-Raphson shooting algorithm. In Fig. 2 we show all poles of $T_{\tilde{J}}$ up to energies of 11.2 GeV. To propagate the statistical errors of the lattice data we generated 1000 statistically independent samples and repeated our computations on each of the samples. For each bound state and resonance there is a differently colored dot in Fig. 2 corresponding to one of the 1000 samples. Bound states are located on the real axis below the $\bar{B}^{(*)}B^{(*)}$-threshold, while resonances are above this threshold and have a non-vanishing imaginary part. The pole positions E of $T_{\tilde{J}}$ are related to masses and decay width via $m = \mathrm{Re}(E)$ and $\Gamma = -2\,\mathrm{Im}(E)$.

In Table 2 we compare our results with experimentally found bound states and resonances. The first 4 states we find for the S-wave ($\tilde{J} = 0$) are reasonably close to the masses of $\Upsilon(1S)$, $\Upsilon(2S)$, $\Upsilon(3S)$ and $\Upsilon(4S)$. Our resonance mass for $n = 5$ is quite similar to the experimental result for $\Upsilon(10753)$, which was recently observed at Belle [7]. The next resonance ($n = 6$) also compares well with the experimentally observed $\Upsilon(10860)$. For $\Upsilon(11020)$ on the other hand there is no match with our theoretical results. The closest resonance we find ($n = 7$) is already in the region where our results can not be trusted anymore.
For $\tilde{J} = 1$ all the bound states we find are reasonably close to the experimentally observed states. There are unfortunately no experimental results for resonances in this sector.
For the D wave we find a bound state ($n = 1$) very close to the experimentally observed $\Upsilon(1D)$. The $\Upsilon(11020)$ resonance could also be a D-wave state but the closest resonance we find ($n = 3$) is in the region where our results can not be trusted anymore.
For $\tilde{J} = 3$ there are no experimentally observed states in this sector yet.
We expect, that our results still have systematic errors of the magnitude of 50-100 MeV. The main error sources are neglecting heavy spin effects and $B - B^*$ mass splitting. We also lack more suitable lattice QCD data for static potentials.

7. Conclusion

We found bound states and resonances for S, P, D and F wave bottomonium up to 11 GeV which compare reasonably to the already experimentally observed states. In particular we obtained states

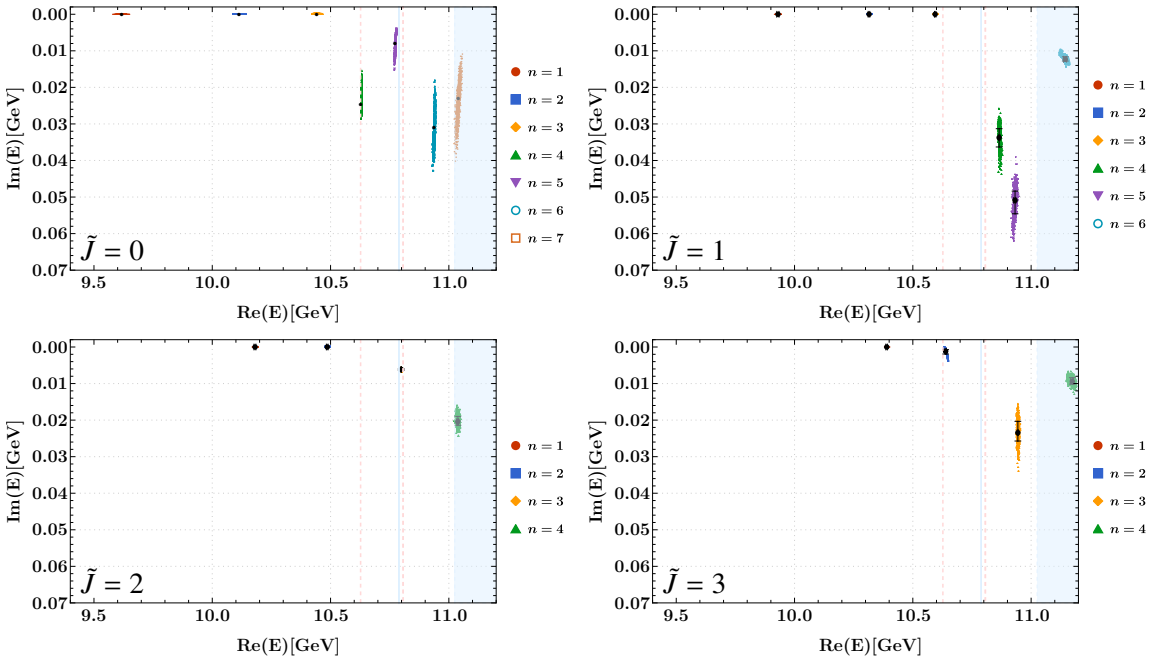

Figure 2: Positions of the poles in the complex plane of $T_{\tilde{J}}$ including the $\bar{B}_s^{(*)} B_s^{(*)}$-channel for all bound states and resonances below 11.2 GeV for angular momentum $\tilde{J} = 0, 1, 2, 3$. Colored point clouds represent 1000 resampled sets of lattice QCD correlators. Black points and bars indicate the mean values and errors. The vertical dashed lines indicate the spin-averaged $\bar{B}^{(*)} B^{(*)}$- and $\bar{B}_s^{(*)} B_s^{(*)}$-thresholds at 10.627 GeV and 10.807 GeV respectively. The light blue shaded region above 11.025 GeV marks the opening of the threshold of one heavy-light meson with negative parity and another one with positive parity. Any results in this region can not be trusted anymore.

that match the experimentally found resonances $\Upsilon(10750)_{\text{BELLE II}}$ and $\Upsilon(10860)$. Unfortunately, we were not able to make a statement, whether $\Upsilon(11020)$ is an S or D wave state yet. We were able to make predictions for many bound states and resonances with $\tilde{J} > 0$ which may be found in the future by the experiment. Our long-term goal is to reduce systematic errors as much as possible to be able to predict bound states and resonances for the experiment. Our next step will be to perform a dedicated lattice QCD computation of the static potentials and the future we will also work on including heavy spin effects and $B - B^*$ mass splitting.

References

[1] G. S. Bali *et al.* [SESAM], Phys. Rev. D **71**, 114513 (2005) doi:10.1103/PhysRevD.71.114513 [arXiv:hep-lat/0505012 [hep-lat]].

[2] M. Born and R. Oppenheimer, Annalen der Physik 389, 457 (1927).

[3] P. Bicudo, M. Cardoso, A. Peters, M. Pflaumer and M. Wagner, Phys. Rev. D **96**, no.5, 054510 (2017) doi:10.1103/PhysRevD.96.054510 [arXiv:1704.02383 [hep-lat]].

[4] S. Prelovsek, H. Bahtiyar and J. Petkovic, Phys. Lett. B **805**, 135467 (2020) doi:10.1016/j.physletb.2020.135467 [arXiv:1912.02656 [hep-lat]].

from poles of $T_{\tilde{J}}$				from experiment			
$\tilde{J}^{PC}$	n	Re(E)[GeV]	Γ[MeV]	name	m[GeV]	Γ[MeV]	$I^G(J^{PC})$
0^{++}	1	9.618^{10}_{15}	-	$\eta_b(1S)$	9.399(2)	10(5)	$0^+(0^{+-})$
				$\Upsilon_b(1S)$	9.460(0)	≈ 0	$0^-(1^{--})$
	2	10.114^{7}_{11}	-	$\eta_b(2S)_{\text{BELLE}}$	9.999(6)	-	$0^+(0^{+-})$
				$\Upsilon(2S)$	10.023(0)	≈ 0	$0^-(1^{--})$
	3	10.442^{7}_{9}	-	$\Upsilon(3S)$	10.355(1)	≈ 0	$0^-(1^{--})$
	4	10.629^{1}_{1}	$49.3^{+5.4}_{-3.9}$	$\Upsilon(4S)$	10.579(1)	21(3)	$0^-(1^{--})$
	5	10.773^{1}_{2}	$15.9^{+2.9}_{-4.4}$	$\Upsilon(10750)_{\text{BELLE II}}$	10.753(7)	36(22)	$0^-(1^{--})$
	6	10.938^{2}_{2}	$61.8^{+7.6}_{-8.0}$	$\Upsilon(10860)$	10.890(3)	51(7)	$0^-(1^{--})$
	7	11.041^{5}_{7}	$45.5^{+13.5}_{-8.2}$	$\Upsilon(11020)$	10.993(1)	49(15)	$0^-(1^{--})$
1^{--}	1	9.9302^{43}_{52}	-	$\chi_{b0}(1P)$	9.859(1)	-	$0^+(0^{++})$
				$h_b(1P)$	9.890(1)	-	$?^?(1^{+-})$
				$\chi_{b1}(1P)$	9.893(1)	-	$0^+(1^{++})$
				$\chi_{b2}(1P)$	9.912(1)	-	$0^+(2^{++})$
	2	10.3152^{29}_{40}	-	$\chi_{b0}(2P)$	10.233(1)	-	$0^+(0^{++})$
				$\chi_{b1}(2P)$	10.255(1)	-	$0^+(1^{++})$
				$h_b(2P)_{\text{BELLE}}$	10.260(2)	-	$?^?(1^{+-})$
				$\chi_{b2}(2P)$	10.267(1)	-	$0^+(2^{++})$
	3	10.5944^{32}_{28}	-	$\chi_{b1}(3P)$	10.512(2)	-	$0^+(0^{++})$
	4	10.8648^{37}_{21}	$67.5^{+5.1}_{-4.9}$				
	5	10.9321^{33}_{54}	$101.8^{+7.3}_{-5.1}$				
	6	11.1444^{52}_{75}	$25.0^{+1.1}_{-1.3}$				
2^{++}	1	10.1809^{35}_{46}	-	$\Upsilon(1D)$	10.164(2)	-	$0^-(2^{--})$
	2	10.4861^{32}_{36}	-				
	3	11.0380^{30}_{44}	$40.8^{+2.0}_{-2.8}$				
3^{--}	1	10.3898^{28}_{39}	-				
	2	10.6388^{31}_{25}	$2.4^{+1.5}_{-0.9}$				
	3	10.9440^{20}_{29}	$46.8^{4.6}_{6.2}$				
	4	11.1740^{51}_{69}	$1.9^{+2.1}_{-1.4}$				

Table 2: Masses and decay widths for $I = 0$ bottomonium from the coupled channel Schroedinger equation (20). For comparison we also list available experimental results. The $\bar{B}^{(*)}B^{(*)}$- and $\bar{B}_s^{(*)}B_s^{(*)}$-threshold are marked by dashed lines. Errors on our results are purely statistical.

[5] J. Bulava, B. Hörz, F. Knechtli, V. Koch, G. Moir, C. Morningstar and M. Peardon, Phys. Lett. B **793**, 493-498 (2019) doi:10.1016/j.physletb.2019.05.018 [arXiv:1902.04006 [hep-lat]].

[6] P. Bicudo, N. Cardoso, L. Müller and M. Wagner, Phys. Rev. D **103**, no.7, 074507 (2021) doi:10.1103/PhysRevD.103.074507 [arXiv:2008.05605 [hep-lat]].

[7] R. Mizuk *et al.* [Belle], JHEP **10**, 220 (2019) doi:10.1007/JHEP10(2019)220 [arXiv:1905.05521 [hep-ex]].

[8] P. Bicudo, M. Cardoso, N. Cardoso and M. Wagner, Phys. Rev. D **101**, no.3, 034503 (2020) doi:10.1103/PhysRevD.101.034503 [arXiv:1910.04827 [hep-lat]].